






Article

Ultra-Short Pulse Laser Cleaning of Contaminated Pleistocene Bone: A Comprehensive Study on the Influence of Pulse Duration and Wavelength

Md. Ashiqur Rahman ^{1,2,3}, Germán F. de la Fuente ^{1,*} , José Miguel Carretero ⁴, M^a Pilar Alonso Abad ² , Rodrigo Alonso Alcalde ⁵ , Rémy Chapoulie ⁶, Nick Schiavon ³  and Luis A. Angurel ¹ 

¹ Instituto de Nanociencia y Materiales de Aragón (CSIC—University of Zaragoza), c/María de Luna 3, 50018 Zaragoza, Spain

² Área de Historia del Arte and Unidad Asociada de I+D+i al CSIC “Vidrio y Materiales del Patrimonio Cultural (VIMPAC)”, Departamento de Historia, Geografía y Comunicación, Universidad de Burgos, Pº Comendadores S/N, 09001 Burgos, Spain

³ HERCULES Laboratory, University of Évora, Largo Marquês de Marialva 8, 7000-809 Évora, Portugal

⁴ Laboratorio de la Evolución Humana and Unidad Asociada de I+D+i al CSIC “Vidrio y Materiales del Patrimonio Cultural (VIMPAC)”, Departamento de Historia, Geografía y Comunicación, Universidad de Burgos, Plaza Misael Bañuelos S/N, 09001 Burgos, Spain

⁵ Área de Didáctica y Dinamización, Museo de la Evolución Humana, Paseo Sierra de Atapuerca nº2, 09002 Burgos, Spain

⁶ Archéosciences Bordeaux UMR 6034, CNRS, University Bordeaux Montaigne, 33607 Pessac, France

* Correspondence: german.delafuente.leis@csic.es

Abstract: The impact of wavelength and pulse duration in laser cleaning of hard blackish contaminants crust from archaeologically significant Pleistocene bone is investigated in this research. The objective is to determine the practical cleaning procedures and identify adequate laser parameters for cleaning archaeological bone from *Sima de los Huesos* (Spain) based on conservation and restoration perspectives. Bone surface cleaning was performed utilizing two Q-switched Nd:YAG lasers: sub-nanosecond pulsed lasers with emission wavelengths at 355 nm and 1064 nm, respectively, and a Yb:KGW femtosecond pulsed laser with an emission wavelength in the third harmonic at 343 nm. In all experiments, the laser beam scanning mode was applied to measure cleaning efficiency in removing contaminants and degradation products while assessing the underlying substrate surface damage. Several properties, including wavelength-dependent absorption, pulse repetition rate, and thermal properties of the material, are analyzed when evaluating the ability of these lasers to boost the cleaning efficiency of the deteriorated bone surface. Bone surface morphology and composition were studied and compared before and after laser irradiation, using Optical Microscopy, Scanning Electron Microscopy with Energy Dispersive X-ray Spectrometry (SEM-EDS), Fourier Transform Infrared Spectroscopy (FTIR), and X-ray Photoelectron Spectroscopy (XPS) characterization methods. The results indicate that 238-femtosecond UV laser irradiation with 2.37 TWcm^{-2} is significantly safer and more efficient toward surface contaminant desorption than sub-nanosecond laser irradiation. The results herein presented suggest that these types of fs lasers may be considered for realistic laser conservation of valuable historic and archaeological museum artifacts.

Keywords: femtosecond laser; sub-nanosecond laser; cleaning; pulse duration; wavelength; archaeological bone; *Sima de los Huesos*



Citation: Rahman, M.A.; de la Fuente, G.F.; Miguel Carretero, J.; Abad, M.P.A.; Alcalde, R.A.; Chapoulie, R.; Schiavon, N.; Angurel, L.A. Ultra-Short Pulse Laser Cleaning of Contaminated Pleistocene Bone: A Comprehensive Study on the Influence of Pulse Duration and Wavelength. *Heritage* **2023**, *6*, 2503–2519. <https://doi.org/10.3390/heritage6030132>

Academic Editor: Moira Bertasa

Received: 31 December 2022

Revised: 7 February 2023

Accepted: 23 February 2023

Published: 26 February 2023



Copyright: © 2023 by the authors. Licensee MDPI, Basel, Switzerland. This article is an open access article distributed under the terms and conditions of the Creative Commons Attribution (CC BY) license (<https://creativecommons.org/licenses/by/4.0/>).

1. Introduction

Conservation of cultural heritage (CH) artefacts includes solving problems that are currently causing their deterioration, as well as preventing and/or diminishing further damage. Given the wide diversity of materials, surface textures, and deterioration processes found in CH objects, the appropriateness of any conservation approach should be

thoroughly examined and verified for each kind. Removing contaminants from artifacts without affecting the outermost substrate layer is an essential prerequisite for a successful conservation process. For artifact cleaning, laser ablation techniques are considered a complementary alternative to conventional mechanical or chemical procedures and are expected to have a considerable impact on conservation operations in the near future. These are under continuous improvement, in parallel with laser technology evolution, to eventually succeed in cleaning such artifacts [1–4]. Laser ablation has been applied on a wide range of archaeological materials, including stones, ceramics, paintings, metals, monuments, bones, parchment, textiles, etc., [5–12].

A laser cleaning approach relies on the selective ablation of degradation and pollutant products from surfaces, and it has the added benefit of being non-contact, chemical-free, and environmentally friendly. Several parameters of laser systems, including their wavelength [13], pulse duration, and peak power are defined by the operator [14]. In general, these parameters can be adjusted to remove polluted and deteriorated layers with high efficiency while causing no visible or detectable alteration to the original sample substrate surface [15]. The degree of selectivity and precise, gradual removal of contaminants are among the most relevant advantages of this technique [16,17]. Additionally, automated laser cleaning is an attractive alternative that has long been envisioned [18,19].

The laser emission wavelength interaction and its influence on the removal of contaminants from surfaces have been the subject of several investigations which also assessed the original substrate preservation [15,16,19,20]. A large variety of contaminants and substrate compositions are encountered in Cultural Heritage materials. Laser parameter optimization hypotheses assert that the irradiance value of the laser beam, the absorptivity of the materials, and the thermal conductivity of the layer being removed are all crucial in the safe and successful removal of contaminated layers, and all of these have a direct relationship with the proper selection of the wavelength [15,16,19].

Pulse duration has a significant impact on laser cleaning. Archaeologically important materials have been cleaned using lasers with a microsecond (μs) to femtosecond (fs) pulse duration [21–25]. When shorter pulses are used, heat accumulation and local temperature increase are both significantly reduced [26,27]. High-precision laser intervention is now possible because of the advent of lasers with short and ultra-short pulse duration. Lasers with pulse duration in the picosecond (ps) to femtosecond (fs) range, for example, exhibit a substantial improvement in micromachining quality for a variety of materials [28].

Furthermore, ultrashort pulse (<sub-ns) laser systems developed in recent years have been demonstrated applicable in the field of heritage conservation [29–31]. In comparison to nanosecond pulsed lasers, ultrashort laser pulses exhibit intense nonlinear interactions with matter as one of their most striking features [32,33]. The comparatively low thermal load generated by ultrashort laser pulses on the substrate reduces any collateral impact caused by heat accumulation [34,35], such as burning, cracking, and thermally induced chemical changes. Additionally, the nonlinearity of the interaction makes it possible to remove nanometric thin layers of material with great precision and control [27,36].

Laser cleaning of archaeological artifacts has increased considerably, taking advantage of their controllability, accuracy, straightforwardness, and working capacity in all material types [37–43]. Despite the fact that lasers have been successfully applied to clean archaeological materials with various forms of pollution and/or degradation during the last three decades, conservators have paid little attention to laser cleaning of archaeological mineralized bone, as there have not been many case studies published on the subject [37,44,45]. The major cause for this might be a lack of suitable pulse lasers that protect delicate and fragile surfaces from cleaning instrument-produced damages. It's possible that the inconsistent composition and pace of bone breakdown and mineralization is another major reason why laser bone cleaning of archaeological significance has received so little study.

The objective of this work is to explore the use of ultra-short pulsed lasers to achieve surface desorption of bones excavated from the *Sima de los Huesos* archaeological site at *Sierra de Atapuerca* (Burgos, Spain) [46,47]. Most important during this work is to establish

laser irradiation parameters that help avoid damage and retain the anatomical information hidden by bone deterioration and surface contamination that has occurred during the long historic period since their burial. Hard dirt, sediment, bacteria, and other forms of organic and inorganic substances are all examples of potential bone contaminants due to long burial periods. These contaminants, if not eliminated, might affect the bone's appearance and chemical composition, leading to erroneous conclusions about the bone's age, origin, and other aesthetic characteristics. Moreover, contaminants can bring modern elements into ancient specimens, making it challenging to identify the authenticity of the bones and acquire trustworthy scientific conclusions. This is why cleaning up archaeological bone is essential to ensuring their continued scientific integrity [48,49].

2. Materials and Methods

2.1. Materials

Three Pleistocene pieces from a single bear rib bone were selected for this study. They are physically defined as follows: (i) 2.6 cm long \times 1.2–1.4 cm wide \times 0.7–0.85 cm thick (Figure 1a), (ii) 1.9 cm long \times 0.6 cm wide \times 0.2 cm thick (Figure 1b), and (iii) 2.5 cm long \times 0.7–1.0 cm wide \times 0.4 cm thick (Figure 1c). This 430,000-year-old rib bone was excavated in 1986 as soiled material with atmospheric dust on its surface. It had been previously cleaned mechanically with a soft brush, in order to remove any loose debris as a preliminary step toward conservation. Large areas of these bone artifacts exhibit varied shades of hard blackish-yellowish stains and encrustations unevenly distributed, in contrast to the normal whitish-yellowish color associated with fossilized bones, which most likely arise from weathering patterns attributed to Fe staining and Mn mineralization effects [50,51]. The purpose of the present study is to clean the hard-blackish-yellowish stains and encrustations from the outermost layer of this bone without changing its natural appearance.

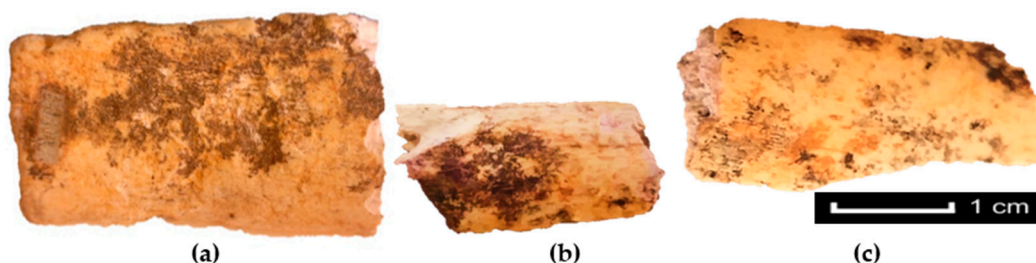


Figure 1. Bear rib (shaft) bone pieces were excavated in the *Sima de los Huesos* archaeological site (Burgos, Spain); photographs show the front side perspectives of the bone fragments (a–c) subjected to study in this work.

2.2. Laser Cleaning Systems and Parameters

Reference laser parameters that will be used for convenient comparisons between the three different lasers employed in this study are defined as follows. Energy per pulse (E_p) is calculated by dividing the energy stored in the laser cavity per second over the pulse repetition frequency (f). Fluence F_{pulse} is the energy density per pulse and is calculated by dividing E_p over the laser beam cross-section area, determined using the $1/e^2$ criteria [52]. Irradiance I_{pulse} , on the other hand, is calculated by dividing the fluence over the pulse duration, τ .

Laser interventions were performed using three different laser systems (Table 1):

- (i) Ultraviolet (UV) irradiation was carried out at 343 nm using the linearly polarized output of an fs laser system (Carbide model, Light Conversion, Lithuania), coupled with a galvanometer mirror beam steering apparatus with final output through a 330 mm focal length telecentric lens (Direct Machining Control, UAB, Vilnius, Lithuania). Irradiation experiments were carried out with a pulse duration of 238 fs, a maximum output power of 9.33 W, and a Gaussian beam profile diameter of 30 μm .

The pulse repetition rate could be adjusted between 1 kHz and 1 MHz, using a pulse peak divider (PPD) option.

- (ii) An air-cooled 800 ps pulsed 8 W (40 μJ max. E_p) sub-ns near-infrared (n-IR) laser (PowerLine Pico 10-1064, ROFIN-SINAR Laser GmbH, Germany) emitting at a wavelength of 1064 nm, integrated into a galvanometer mirror apparatus fitted with a 160 mm focal length flat-field lens, was employed as a second system. The beam waist diameter was determined as 80 μm . Its pulse repetition rate ranged between 200 and 800 kHz.
- (iii) The third system employed was a 3 W, air-cooled third harmonic solid-state laser with emission at 355 nm, a pulse duration of 300 ps, and a maximum output pulse energy of 15 μJ (PowerLine Pico 10-355 from ROFIN-SINAR Laser GmbH, Germany). This laser was also integrated into a galvanometer mirror system fitted with a 160 mm focal length flat-field lens, which resulted in an elliptical beam, with a waist axis of 34 μm and 29 μm . The pulse repetition rate was selectable between 200 and 800 kHz.

A continuous laser beam scanning approach [53] was applied to selectively irradiate specific localized sample areas, as described in detail in [5,49].

Table 1. Emission parameters of the lasers used in this investigation. Values are given for the pulse emission wavelength (λ), average power (P), pulse duration (τ), pulse repetition rate (f), maximum pulse energy (E_p), and distance between adjacent laser scanning lines d and beam waist (D_b) applying the $1/e^2$ criterion for a gaussian beam distribution [52].

Emission Characteristics	Femtosecond (fs) Laser	Sub-Nanosecond Laser	Sub-Nanosecond Laser
Wavelength λ	343 nm	1064 nm	355 nm
Pulse duration τ	238 fs	800 ps	300 ps
Pulse repetition rate f	200 kHz–1 MHz	200–800 kHz	200–800 kHz
Max. average power P	9.33 W	8 W	3 W
Max. pulse energy E_p	46.6 μJ	40 μJ	15 μJ
Beam diameter D_b	30 μm	80 μm	34 μm (2a) \times 29 μm (2b)
Distance between laser passes d	15 μm	20 μm	20 μm

A series of initial explorative experiments were conducted using both fs and sub-ns laser sources to determine the most appropriate parameters for the removal of contaminants and degradation products, taking into consideration prior research on ancient bones [5,37,44]. The target was irradiated evenly with the sub-ns laser throughout a $2 \times 2 \text{ mm}^2$ area in the X direction along parallel lines. On the other hand, fs laser irradiation of a comparable region was accomplished by first scanning the beam along parallel X-axis lines and then crossing Y-axis lines in a perpendicular direction. Bidirectional hatching with no outline mode was applied in all cases.

Thermal incubation, or the accumulation of energy input over time into a specific region of the sample, must be controlled by defining E_p and the ratio of pulse repetition rate to beam scan speed. The latter allows for defining spot-to-spot physical overlap and pulse-to-pulse time overlap. Irradiance (power density per laser pulse) and fluence (energy density per laser pulse) are not proportional in this study because three distinct laser pulse duration values are employed. Irradiance was chosen as the comparative reference here, since its values are independent of laser pulse duration and indirectly affect heat accumulation on the irradiated material [5,49].

2.3. Characterization Techniques

Bone surface elemental composition, morphology, and microstructure were investigated before and after the laser treatment. High-resolution imaging was achieved using a Quanta FEG250 Environmental Scanning Electron Microscope (ESEM). EDS (EDAX Genesis) was used to evaluate the elemental composition semi-quantitatively at 10 kV electron

acceleration voltages, while all obtained values were standardized to a non-laser treated portion of the same area of the sample.

In order to obtain FTIR spectra, a single reflection diamond ATR module and a Brüker Alpha spectrometer were utilized. Background measurements were taken prior to bone sample analysis in order to decrease the impact of carbon dioxide and water vapor on the results. As a consequence of being in direct touch with the diamond crystal, which was positioned on the surface of the sample holder, the bone surface was subjected to pressure. The spectra obtained in the absorbance mode with 128 scans and a spectral resolution of 4 cm^{-1} were acquired within the 4000 to 375 cm^{-1} range. The OPUS/Mentor program (version 6.5) was used to record and analyze the spectra. Identification of bone composition was accomplished by comparing the major characteristics of the acquired spectra between untreated and laser-treated surfaces, as well as with those from the published literature that have made use of comparable methods and materials.

The chemical composition of the outermost bone surface was determined using an X-ray photoelectron spectrometer (Kratos AXIS Supra XPS, monochromatic Al K X-ray source with 225 W : $8\text{ mA}/15\text{ kV}$ energy). With a starting pressure of 10^{-9} Torr and a measurement area of $700\text{ }\mu\text{m} \times 300\text{ }\mu\text{m}$, the photoelectron signal for the complete survey spectrum was collected. The pass energy values for each step were as follows: (i) Wide: $160\text{ eV}/1000\text{ meV}$; (ii) Regions: $20\text{ eV}/100\text{ meV}$. To minimize sample charging effects, all samples were pretreated using a combination of electron and argon ion gun neutralizer systems (Ar^+ 500 eV). The bone sample was analyzed at a depth of roughly 5 nm ($3\text{--}10\text{ nm}$) in many areas. The hybrid-slot lens mode was used to collect spectra for the broad survey scan and particular places of interest, resulting in a spot analysis area of about $700\text{ nm} \times 300\text{ nm}$. Analyses were conducted before and after 300 s of Ar^+ etching.

The bone surfaces were examined using a $230\times$ magnification handheld microscope (Dino-Lite Edge) connected to a computer via USB. The final image was recorded using the Dino Capture 2.0 operating software. A thermal imaging camera (Therma Cam P25, Teledyne FLIR Systems, USA) was utilized to record an increase in the bone surface average temperature while it was irradiated.

3. Results and Discussion

The damage threshold of the bone is identified by the irradiance value at which surface changes, such as melting, color changes, cracking, spallation, or extraction become visible under the optical microscope and SEM investigation. Particular attention was focused on changes detected in the Ca/P compositional ratio, as it indicates when the bone substrate is reached and bone optical absorption properties are observed [54]. Selected areas of the final surface were locally irradiated during several scanning cycles, in order to fine-tune the progressive removal of contaminant layers from the bone surface. The degree of interaction between the laser and the bone substrate, and therefore the degree of damage to the latter, is determined by a combination of irradiance and incubation values [55]. In order to adequately analyze melting evidence, and color and microstructural changes, small portions of the surface were irradiated throughout various regions of the bone and initially investigated and, respectively examined by optical and electron microscopy.

3.1. Application of Sub-Ns n-IR and UV Laser

Multiple observations of sub-ns n-IR laser cleaning led to the conclusion that irradiation levels below $\approx 0.40\text{ GWcm}^{-2}$ ensure that bone damage is avoided. Additionally, these results indicated that damage to the substrate surface occurred at an irradiation level of 0.45 GWcm^{-2} (Figures 2b and 3: Area 4). As a result, and with a safety margin in mind, irradiation values less than 0.40 GWcm^{-2} appear to cause no harm and were so chosen for further irradiation fine-tuning.

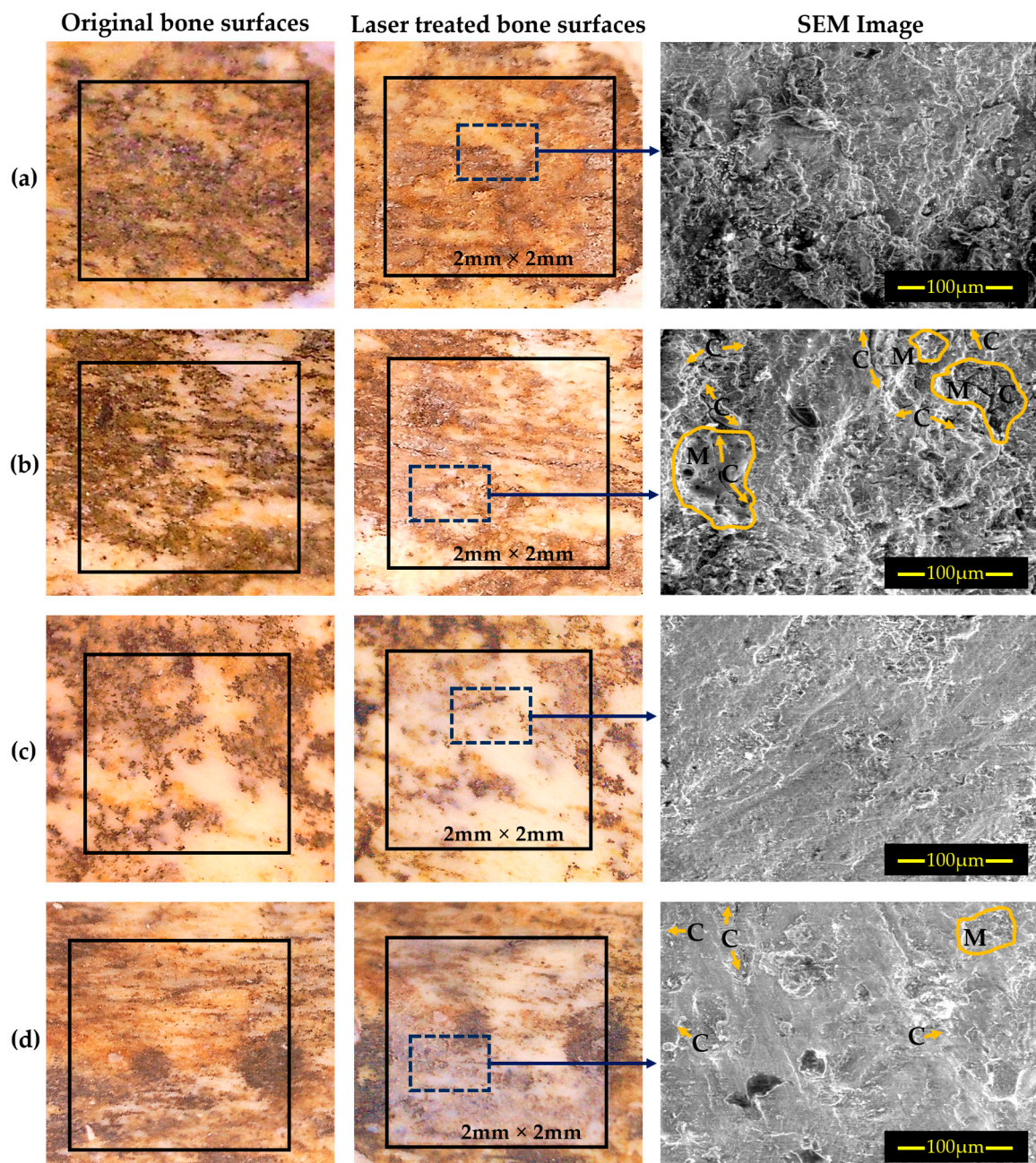


Figure 2. Optical microscopy images of the original bone region (**left**), laser beam scan mode treated bone region (**middle**), and corresponding SEM images of the laser cleaned area. (**a,b**) presents the sub-ns n-IR laser treatment while (**c,d**) shows the outcomes of sub-ns UV laser treatment. Evidence of cracks and melting is indicated by yellow arrows and represented by letters 'C' and 'M' accordingly.

When the laser irradiance level is increased, the average bone surface temperature rises. Quantification of accumulated heat was considered important mainly when irradiating the bone surface with the n-IR wavelength, as heating did not appear so relevant in the case of UV laser irradiation. Nonetheless, a comparative study between the three laser emissions reported here is presently underway. Figure 3 thus depicts the average temperature increase due to the heat accumulated when the bone surface is irradiated with an 800 ps n-IR laser. Using the processing parameters listed in Table 2, it takes roughly 1.5 s to treat an area of 2 mm² of the bone surface just once. IR thermal camera's measuring range of −40 °C to 125 °C is exceeded by the maximum temperature for 0.45 GWcm^{−2} irradiance values (Figure 3: Area 4). At a temperature of more than 125 °C, melt and cracks on the

bone surface started to appear. It was observed, however, that irradiation parameters in the vicinity of the cleaning threshold induce a temperature rise to a maximum value of $\approx 123^\circ\text{C}$, while the ablation threshold can induce maximum temperatures approaching 75°C (Figure 3: Area 1).

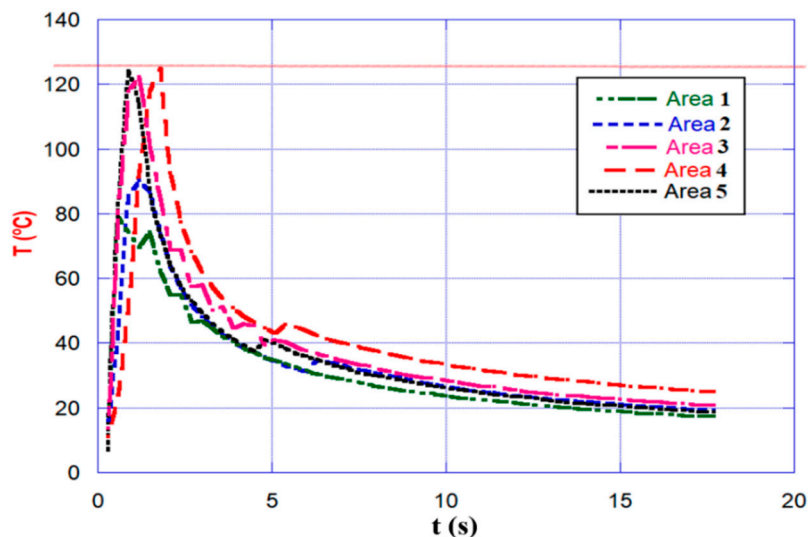


Figure 3. Average temperature changes recorded with a Therma Cam P25 IR camera during 800 ps 1064 nm n-IR laser irradiation of bone samples, reported in Figure 2 and Table 2.

However, after conducting several irradiation experiments, it was determined that the cleaning effectiveness was insufficient for eliminating this sort of hard-blackish-yellowish stains and encrustations. On the other hand, when the number of treatment cycles increased, limited melting began to occur and fractures became visible. For all of these trials, the spatial energy distribution was kept constant, as was the ratio of scanning speed to repetition rate, as indicated in Table 2. Irradiation was concentrated on the sample’s dark blackish regions as seen in Figure 1a.

Table 2. Interaction of sub-ns lasers with Pleistocene bone, studied and reported for the indicated experimental parameters. The distance between two lines was fixed at $20\ \mu\text{m}$, and the number of irradiation cycles was fixed at 1 in all experiments.

Laser	Area	P (W)	f (kHz)	E_p (μJ)	v (mm/s)	F_{pulse} (J/cm^2)	I_{pulse} (GW/cm^2)	Observations
Sub-ns n-IR (1064 nm) 800 ps Laser	1	7.24	700	10.3	7000	0.20	0.25	Very little cleaning (Figure 3: Area 1). Cleaning efficiency is not good
	2	7.24	600	12.1	6000	0.24	0.30	(Figures 2a and 3: Area 2). Cleaning efficiency is not good
	3	7.24	500	14.5	5000	0.28	0.36	(Figure 3: Area 3).
	4	7.24	400	18.1	4000	0.36	0.45	Micro-cracks and melt evidence observed (Figures 2b and 3: Area 4). Cleaning efficiency is not good
	5	6.29	400	15.7	4000	0.31	0.39	(Figure 3: Area 5).
Sub-ns UV (355 nm) 300 ps Laser	1	0.58	300	1.9	3000	0.25	0.83	Cleaning efficiency is not much appreciable.
	2	0.49	500	1.0	5000	0.12	0.42	No noticeable cleaning.
	3	0.66	400	1.7	4000	0.21	0.71	Cleaning efficiency is not good.
	4	0.90	300	3.0	3000	0.38	1.29	Structural damages, melt evidence and color changes observed (Figure 2d).
	5	1.02	400	2.6	4000	0.32	1.09	Good cleaning (Figure 2c).

According to previous studies reported using a sub-ns UV laser, bone damage can be prevented with irradiation levels approaching 1.15 GWcm^{-2} [5,49]. These findings also showed that irradiation of 1.29 GWcm^{-2} caused damage to the substrate's surface (Figure 2d). To be on the safe side, radiation values less than or equal to $\sim 1.15 \text{ GWcm}^{-2}$ were chosen here for bone irradiation studies, since they appear to cause no harm on the bone surface. It was discovered, however, following several irradiation experiments, that the cleaning efficiency was insufficient for eliminating the hard, black encrustations and colored stains. As expected, an increase in the number of irradiation cycles with the same settings resulted in cracks becoming evident and colors observed to change. The scanning speed to repetition rate ratios was maintained during all of these experiments, as shown in Table 2.

With the objective of removing the blackish-yellowish colored overlayers and stains from the bright white colored substrate, a "cleaning" threshold I_{pulse} range for n-IR beam scan irradiation at 1064 nm was identified, though it was observed that cleaning efficiency was not sufficient to be able to define a satisfactory cleaning threshold. By changing the laser system's power output from 4.39 W to 7.24 W, the irradiance levels used for the aforementioned tests increased from 0.25 to 0.39 GWcm^{-2} (Table 2: sub-ns n-IR 800 ps laser). In contrast, in order to remove the dark blackish colored overlayers and blackish-yellowish stains, a "cleaning" threshold irradiance I_{pulse} range for the UV beam scan was determined by changing the power output of the laser (from 0.23 W to 1.39 W). A satisfactory cleaning irradiance was found at around 0.90 to 1.15 GWcm^{-2} , while inefficient cleaning started from 0.71 GWcm^{-2} . In both laser systems, multiple laser irradiation treatment cycles were carried out on the bone surface, in various locations, and under identical irradiance conditions. Apparently, no contamination or staining removal below this cleaning threshold I_{pulse} settings were observed.

To assess the chemical composition of the bone surface, specifically the hard blackish over-layers and blackish-yellowish stains in both, as received and laser-treated surfaces, XPS data (Figure 4) were analyzed to detect the presence of Mn and Fe, besides the other expected elements associated with bone and soil. XPS revealed the sample's surface and vicinity contained Mn, which could have originated not just during mineralization, but also from within the initial bone [5]. Fe and Mn, which are known to display dark stains are also responsible for the black hue seen in the latter [5]. Both characterization methods indicate that Mn and Fe are still present in appreciable amounts within the 0.45 GWcm^{-2} sub-ns n-IR laser irradiated area (Table 2: Area 5). If bone has, in addition, been submerged for an extended length of time and mechanical breakdown or chemical degradation has occurred, Mn and Fe compounds might precipitate to a depth observable in the bone cross-section near the surface. This could result in blackish-yellowish stains and later encrustations on the bone's topmost layer (Figures 2 and 4).

When treated with both sub-ns lasers, the dark black and yellowish contaminated crusts and stains typically discolored into a brownish hue. However, XPS analysis indicates that when adequate cleaning threshold values were used, laser cleaning did not result in substantial compositional changes. The minor brownish color shift noticed on the bone surface has been attributed to the combined heat dissociation of the Mn and Fe compounds. Analogous findings for different areas of sub-ns UV laser treatment revealed that, at I_{pulse} values slightly above the ablation threshold, colored stains and hard blackish encrustation and/or mineralization are not properly removed, whereas only a very thin layer of matrix material can be removed from the over-layers of the bone surface. These are consistent with previous n-IR laser treatment observations within different areas of the artifact (Figure 2).

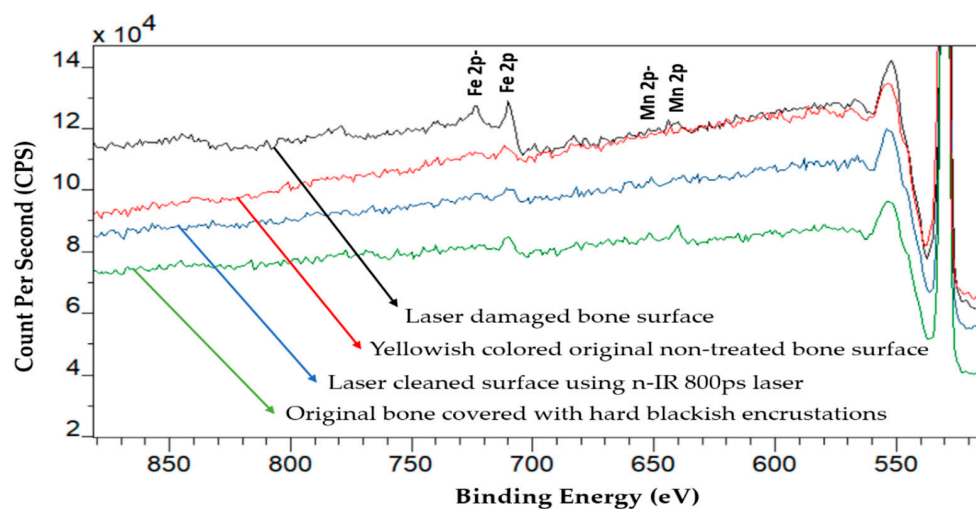


Figure 4. Representative raw XPS survey spectrum of the bear rib bone. Bottom to top: green-colored band obtained from the ‘as received non-treated’ bone; blue-colored band corresponding to the ‘n-IR (1064 nm) 800 ps laser-treated bone surface; red-colored band from the ‘as received non-treated’ bone surface and black-colored band obtained from the laser induced molten surface area of the rib.

3.2. Application of fs UV Laser

In the case of fs UV laser interaction with Pleistocene bone, the interlinear distance was fixed at 15 μm , and the number of irradiation cycles was fixed at 10 for all experiments, carried out in cross-hatch mode (i.e., 0° and 90°). Controlled cleaning of bone with no indication of melting, carbonization, or cracking is possible, as illustrated in Figure 5, utilizing an ultrafast laser with 238 fs pulse duration and emission at a wavelength of 343 nm, even though irradiance values are above that established for the ablation threshold. This is particularly valid when pulse repetition frequencies below 20 kHz are employed [56]. The cleaning operation occurs as a result of the irradiance being above the ablation regime (ca. $<1.24 \text{ TWcm}^{-2}$) for encrustations and stains, ranging in values between ca. 1.24 and 2.79 TWcm^{-2} (Table 3). All of these can be identified in the same original and laser treated areas indicated in the Figure 5.

Table 3. Experimental parameters employed for the initial assessment of fs UV laser interaction with Pleistocene bone, as described in the text.

Area	P (W)	Pulse Frequency f (kHz)	E_p (μJ)	F_{pulse} (J/cm^2)	I_{pulse} (TW/cm^2)	Observations
1	0.42	10	2.1	0.29	1.24	Good cleaning; hard blackish-yellowish encrustations and staining steadily cleaned (Figures 5 and 6: Laser treated Area 1)
2	0.42	10	2.1	0.29	1.24	Good cleaning; hard blackish encrustations and blackish-yellowish staining steadily cleaned (Figures 5 and 6: Laser treated Area 2)
3	0.54	10	2.7	0.38	1.60	Good cleaning; hard blackish encrustations and yellowish staining progressively cleaned (Figures 5 and 6: Laser treated Area 3)
4	0.66	10	3.3	0.46	1.96	Good cleaning; hard blackish encrustations and yellowish staining mostly cleaned (Figures 5 and 6: Laser treated Area 4)
5	0.80	10	4.0	0.56	2.37	Good cleaning; hard blackish encrustations and blackish-yellowish staining mostly cleaned (Figures 5 and 6: Laser treated Area 5)
6	0.94	10	4.7	0.66	2.79	Structural damages observed; hard blackish encrustations and blackish-yellowish staining mostly cleaned (Figures 5 and 6: Laser treated Area 6)

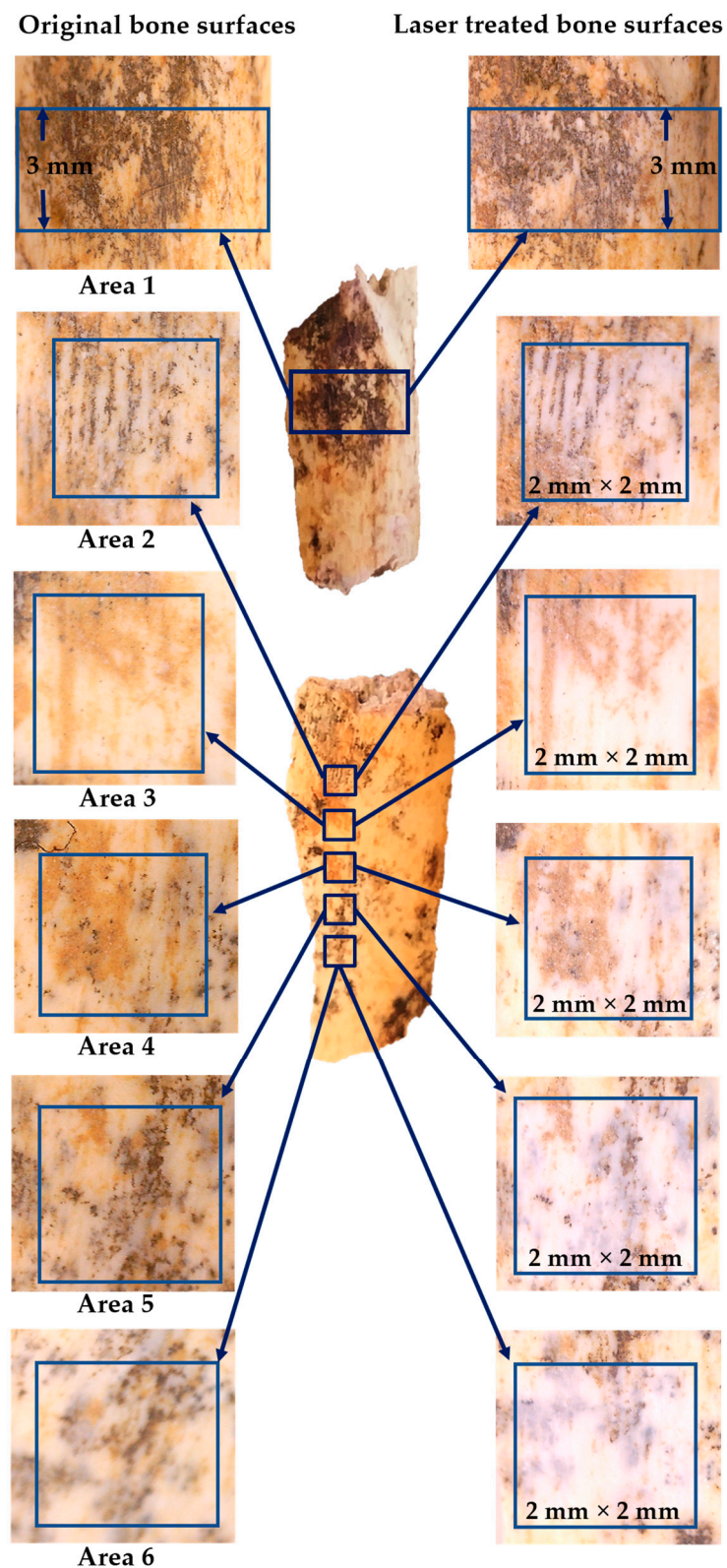


Figure 5. Optical micrographs obtained on the original, as-received archaeological bone artifact (left column) where six areas are identified. An aspect of these same areas after irradiation using a 238 fs laser under the irradiance values given in the text.

According to this study, damage on the bone surface can be avoided at irradiation intensities below 2.37 TWcm^{-2} . Additionally, these data indicated that irradiation at

2.79 TWcm^{-2} produced damage to the substrate's surface, where cracks and melts were evident (Figure 6, Area 6). Irradiance levels at or below 2.37 TWcm^{-2} were thus chosen for further bone laser cleaning experiments, since they appeared to cause no detrimental effect on the bone surface. Following multiple irradiation tests, it was determined that the cleaning efficiency was satisfactory for removing the hard black encrustations and blackish-yellowish staining. By deliberately raising the number of laser beam scan repetitions in cross-scan mode while maintaining the same laser and beam scan parameters, the original appearance of the bone surface was gradually revealed without apparent damage.

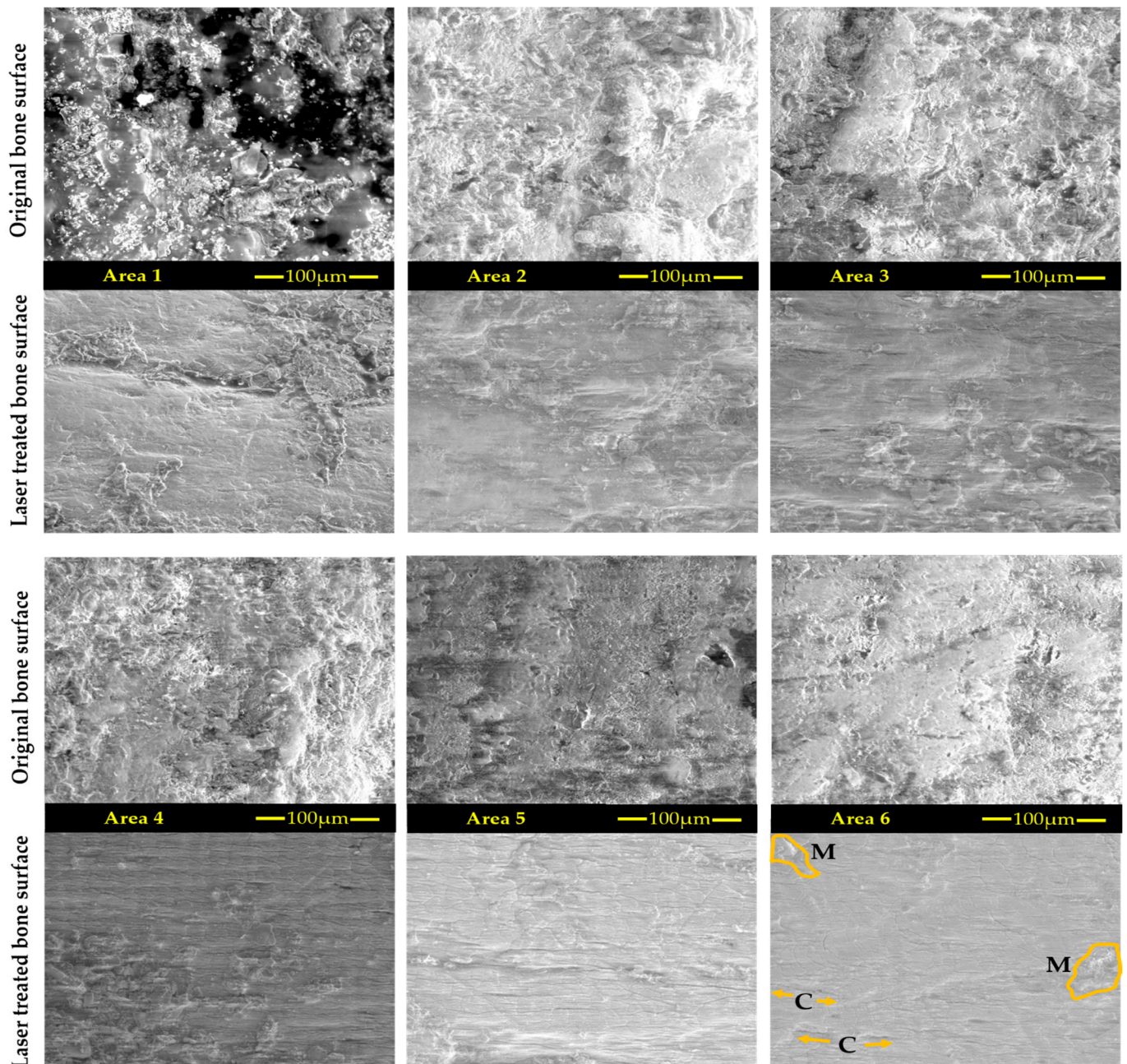


Figure 6. SEM images obtained on the Pleistocene untreated and ‘laser-treated’ bone surfaces subjected to this study. Columns 1 and 3 correspond to areas 1–6, (associated with the left side in Figure 5). Equivalent micrographs are shown in columns 2 and 4, corresponding to laser-treated areas 1–6 (associated with the right side in Figure 5). The letters “C” and “M” in Area 6 denote crack (yellow arrows) and melt (yellow areas) evidence, respectively.

3.3. SEM (EDS) Characterization

The outcomes of fs UV laser beam scan cleaning are shown in Table 3, while Figures 5 and 6 show the outcome of effective good cleaning threshold values and corresponding SEM images. The optical micrographs of Figure 5 show the actual region of the initial, untreated bone (left side), where the blackish mineralized encrustations zone and blackish-yellowish staining are evident; Figure 6 represents the corresponding SEM images, marked as ‘Original bone surface’. The maximum non-damaging laser irradiance values on the sample surface for contaminant removal in dark mineralized areas and blackish-yellowish staining was determined as 2.37 TWcm^{-2} , taking into account a Gaussian pulse spatial beam profile (Table 3, Area 5). The dense blackish-yellowish contaminated crusts and stains did not show any discoloration; similarly, SEM-EDS data (Table 4) indicate that laser cleaning did not alter the composition of the surface under the established satisfactory cleaning conditions for this aforementioned fs laser system.

After fs laser irradiation, the amount of Si, Al, and Fe decreases while the content of Ca and P increases, which is in line with the removal of aluminosilicates and iron-containing compounds measured in the soil found at the burial area (Table 4) [57]. It is also possible that the increased Ca and P content following laser irradiation indicates that those elements are being stabilized by melting, which leads to surface damage, which can be prevented by controlling the laser parameters appropriately. Silicates (i.e., feldspars), nitrates, sulfates, and others may be linked to the burial environment, as these elements are commonly discovered as soil components at archaeological sites, specifically at the *Sierra de Atapuerca* site [57]. As for Fluorine (F) a characteristic component of bone, it has been identified in fossil bones and its concentration has been particularly linked to water intake in the animal’s diet [58,59]; F levels in fossil bones, therefore, vary depending on the location where the fossils are found.

Table 4. Elemental composition of Pleistocene bone surface ‘untreated and after fs laser treatment’ obtained from EDS (SEM) analysis, associated with Figure 6. The presence and distribution of Ca and P, essential components of bone, are confirmed and observed to increase significantly after laser treatment. Mn is observed to increase with laser treatments in all of the analyzed areas. Fe content is found, however, to increase in some areas and decrease in others, as a result of laser treatment. In addition, C-containing contaminants are observed to decrease considerably upon laser irradiation, suggesting that they were abundantly present in the outermost layers of the artifact and that the laser treatment efficiently removes them from the bone substrate.

Elements (wt%)	Area 1	Laser Treated Area 1	Area 2	Laser Treated Area 2	Area 3	Laser Treated Area 3	Area 4	Laser Treated Area 4	Area 5	Laser Treated Area 5	Area 6	Laser Treated Area 6
C	49.1	22.0	15.7	6.7	14.8	7.4	14.9	5.9	12.4	7.2	9.5	6.9
O	26.6	37.3	38.6	34.8	38.9	34.7	38.8	38.0	36.4	35.3	40.6	35.3
Fe	1.4	1.7	5	2.1	5.5	2.0	4.3	5.6	2.8	3.5	4.9	3.5
Na	0.5	0.5	0.5	0.4	0.4	0.5	0.4	0.2	0.5	0.5	0.4	0.4
Mg	0.3	0.3	0.6	0.2	0.6	0.4	0.5	1.0	0.3	0.8	0.5	0.3
Al	2.7	3.2	6.2	2.0	6.3	2.6	4.8	8.6	2.6	5.7	5.8	3.0
Si	3.8	2.9	10.2	3.1	11.5	4.3	7.8	16.9	4.2	10.6	9	4.8
P	3.8	8.9	6.3	14.6	6.0	13.4	8.2	5.7	12.4	9.7	8.8	12.6
K	1.0	0.5	1.9	0.6	2.1	0.9	1.4	2.9	0.8	1.9	1.5	1.0
Ca	10.3	20.5	14.5	33.0	13.3	31.2	18.4	12.6	27.1	21.9	18.5	28.8
Mn	0.5	0.8	0.7	0.9	0.7	0.7	0.5	1.2	0.5	1.2	0.5	1.8

3.4. ATR-FTIR Characterization

Figure 7 depicts the ATR-FTIR spectra of a Pleistocene bear bone in its original excavated condition as well as after it was treated with an fs laser with average irradiances

of 1.24 TWcm^{-2} (Figure 7a) and 2.37 TWcm^{-2} (Figure 7b), respectively. Spectra obtained from treated samples are more indicative of the organic content present within the bone surface, whereas spectra obtained from untreated samples have a lower signal-to-noise ratio. This difference is attributable to the removal of contaminants by the laser, rather than to differences in the bone surface condition.

Phosphate and carbonate absorption bands seen in these spectra represent the mineral phase of bone, which is basically calcium-deficient hydroxyapatite. The most intense bands, related to PO_4^{3-} , emerge at about 1000 and 950 cm^{-1} , respectively, matched to the PO_4^{3-} stretching ν_3 antisymmetric and the ν_1 symmetric modes, respectively. The absorption bands at 1415 and 1450 cm^{-1} correspond to CO_3^{2-} in the B-type PO_4^{3-} and A-type OH^- anionic sites, accordingly. The band at 873 cm^{-1} corresponds to the CO_3^{2-} ν_2 stretching mode [60–63]. Between 1450 and 1750 cm^{-1} , the band of the primary organic constituent of bone, collagen, confirms the presence of organic components [60,61].

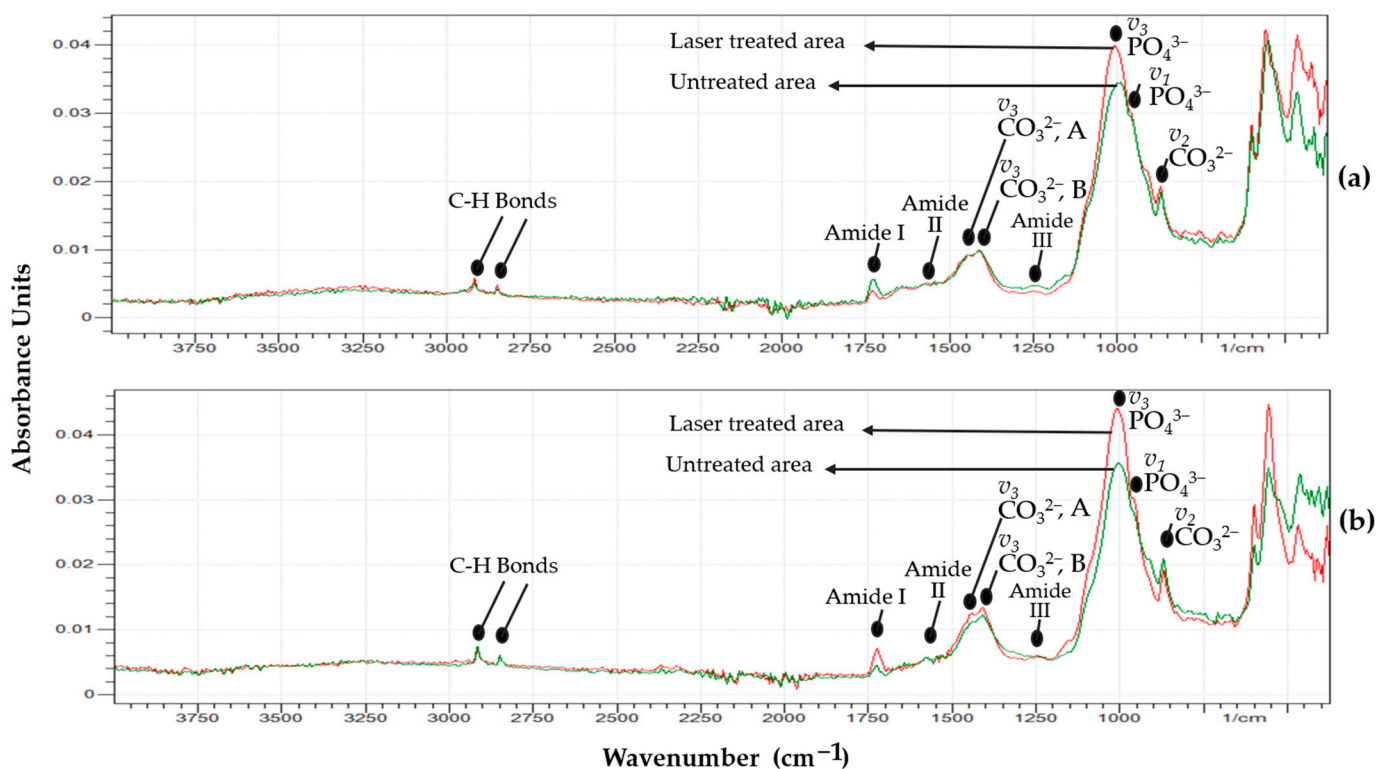


Figure 7. FTIR spectra of fs laser treated and untreated samples, corresponding to the hard blackish contaminated and blackish-yellowish stained surface irradiated with 1.24 TWcm^{-2} (a) and 2.37 TWcm^{-2} (b) along with the untreated original surface area.

The bands at 1690 to 1720 cm^{-1} , 1550 to 1590 cm^{-1} , and 1250 cm^{-1} correspond to the collagen molecule's amide I (C = O bond stretching), amide II (C-N bond stretching and N-H deformation modes), and amide III groups [61]. The wide absorption band at 2920 cm^{-1} is allocated to an amide B group. A collagen group (N-H asymmetric stretching mode), and the peak between 2850 to 2950 cm^{-1} arise from CH_2 chain bond stretching [61–63]. Upon laser irradiation, a closer examination of the spectra indicates that the amide bands are similar or, at least, no significant differences can be identified between the original and laser-treated surfaces. The relative amplitudes of other IR absorption bands, such as those associated with bone mineral, appear to be unaffected by fs laser cleaning.

4. Conclusions

A detailed subsurface investigation of laser intervention using three sub-ns and fs pulsed lasers, in UV and n-IR emission regimes, was carried out in order to assess their po-

tential for cleaning, as well as the appearance of the substrate surface after desorption. The precise damage threshold appears to be independent of the existence of Mn mineralization and Fe staining. The bone surface cleaned with a 1064 nm sub-ns laser generates a significant amount of heat and develops a yellowish hue as a result of significant heat incubation effects, leading to thermomechanical cracking, carbonization, and even necrosis in extreme situations. This wavelength also seems to penetrate the surface without removing all the hard blackish contaminants and blackish-yellowish stains. In contrast, 355 nm sub-ns laser radiation interacts with the bone surface in a very localized, superficial way, making the process impractical from the point of view of its low material removal rate.

Results from a large number of experiments demonstrate that an fs UV laser (343 nm, 238 fs) may be most effective to clean fragile, sensitive archaeologically significant bone surfaces. This laser is quite effective in cleaning bone samples at a cleaning threshold irradiance level of 2.37 TWcm^{-2} , resulting in zero or minimal discoloration, and no distinguishable damage to the bone surface under microscopic examination. When compared with sub-ns lasers, this work revealed that laser pulses with an fs duration can significantly avoid thermal accumulation and facilitate selective removal of contaminants and stains on bone samples. The results herein reported for fs laser cleaning of archaeological bone surfaces had essentially no impact on the substrate's physicochemical characteristics. The use of fs lasers for the removal of blackish encrustations and archaeological bone stains is thus apparently much more adequate and successful than the use of sub-ns lasers.

In essence, ultrafast fs UV lasers are leading-edge instruments that can be highly recommended to complement conventional restoration and conservation methods.

Author Contributions: Conceptualization, M.A.R., G.F.d.l.F., M.P.A.A., R.C., N.S. and L.A.A.; methodology, M.A.R., G.F.d.l.F. and L.A.A.; validation, M.A.R., G.F.d.l.F., J.M.C., M.P.A.A., R.A.A., R.C., N.S. and L.A.A.; formal analysis, M.A.R., G.F.d.l.F. and L.A.A.; investigation, M.A.R., G.F.d.l.F. and L.A.A.; resources, G.F.d.l.F., J.M.C., M.P.A.A., R.A.A. and L.A.A.; data curation, M.A.R., G.F.d.l.F. and L.A.A.; writing—original draft preparation, M.A.R.; writing—review and editing, M.A.R., G.F.d.l.F., J.M.C., M.P.A.A., R.A.A., R.C., N.S. and L.A.A.; visualization, M.A.R., G.F.d.l.F. and L.A.A.; supervision, G.F.d.l.F., M.P.A.A., N.S. and L.A.A.; project administration, N.S., G.F.d.l.F., M.P.A.A. and L.A.A.; funding acquisition, N.S. and G.F.d.l.F. All authors have read and agreed to the published version of the manuscript.

Funding: This research was funded by the H2020-MSCA-ITN-EJD/ED-ARCHMAT action funding under the Marie Skłodowska-Curie grant agreement, No 766311.

Data Availability Statement: Not applicable.

Acknowledgments: The Atapuerca research project is financed by Ministerio de Ciencia, Innovación y Universidades, grant no. PID2021-122355NB-C31/MCIN/AEI/10.13039/501100011033/FED ER.UE. Fieldwork at the Atapuerca sites is funded by the Junta de Castilla y León and the Fundación Atapuerca. The archaeological materials presented in this work were made available by the Laboratory of Human Evolution of the University of Burgos, in close collaboration with the "Colección Museística de Castilla y León" of the Junta de Castilla y León, and Museo de la Evolución Humana (Burgos); we acknowledge Juan Luis Arsuaga for the permit to analyze the sample. The use of Servicio General de Apoyo a la Investigación and the National Facility ELECMI ICTS, node "Laboratorio de Microscopías Avanzadas" at the University of Zaragoza is acknowledged. Partial support was obtained from Departamento de Ciencia, Universidad y Sociedad del Conocimiento of Gobierno de Aragón "Construyendo Europa desde Aragón" (research group T54_20R). This work is part of the ongoing collaboration between INMA (CSIC-University of Zaragoza) and the University of Burgos, under the auspices of Unidad Asociada de I+D+I al CSIC "Vidrio y Materiales del Patrimonio Cultural (VIMPAC)".

Conflicts of Interest: The authors declare no conflict of interest.

References

1. Cooper, M. *Laser Cleaning in Conservation: An Introduction*; Butterworth-Heinemann: Oxford, UK, 1998.
2. Asmus, J.F.; Murphy, C.G.; Munk, W.H. Studies on the Interaction of Laser Radiation with Art Artifacts. In *Developments in Laser Technology II*; SPIE: Bellingham, WA, USA, 1974; Volume 4, pp. 19–30. [[CrossRef](#)]

3. Lahoz, R.; Angurel, L.A.; Brauch, U.; Estepa, L.C.; de la Fuente Leis, G.F. Laser Applications in the Preservation of Cultural Heritage: An Overview of Fundamentals and Applications of Lasers in the Preservation of Cultural Heritage. *Conserv. Sci. Cult. Herit. Appl. Instrum. Anal.* **2013**, 294–332.
4. Nevin, A.; Pouli, P.; Georgiou, S.; Fotakis, C. Laser conservation of art. *Nat. Mater.* **2007**, *6*, 320–322. [[CrossRef](#)] [[PubMed](#)]
5. Rahman, A.; de la Fuente, G.F.; Carretero, J.M.; Maingi, E.M.; Abad, M.P.A.; Alcalde, R.A.; Chapoulie, R.; Schiavon, N.; Angurel, L.A. Sub-ns-pulsed laser cleaning of an archaeological bone from the Sierra de Atapuerca, Spain: A case study. *SN Appl. Sci.* **2021**, *3*, 865. [[CrossRef](#)]
6. Lazzarini, L.; Marchesini, L.; Asmus, J.F. Lasers for the Cleaning of Statuary: Initial Results and Potentialities. *J. Vac. Sci. Technol.* **1973**, *10*, 1039–1043. [[CrossRef](#)]
7. Palomar, T.; Oujja, M.; Llorente, I.; Barat, B.R.; Cañamares, M.; Cano, E.; Castillejo, M. Evaluation of laser cleaning for the restoration of tarnished silver artifacts. *Appl. Surf. Sci.* **2016**, *387*, 118–127. [[CrossRef](#)]
8. Buccolieri, G.; Nassisi, V.; Buccolieri, A.; Vona, F.; Castellano, A. Laser cleaning of a bronze bell. *Appl. Surf. Sci.* **2012**, *272*, 55–58. [[CrossRef](#)]
9. Siano, S.; Agresti, J.; Cacciari, I.; Ciofini, D.; Mascalchi, M.; Osticioli, I.; Mencaglia, A.A. Laser cleaning in conservation of stone, metal, and painted artifacts: State of the art and new insights on the use of the Nd:YAG lasers. *Appl. Phys. A* **2011**, *106*, 419–446. [[CrossRef](#)]
10. Burmester, T.; Meier, M.; Haferkamp, H.; Barcikowski, S.; Bunte, J.; Ostendorf, A. Femtosecond Laser Cleaning of Metallic Cultural Heritage and Antique Artworks. In *Lasers in the Conservation of Artworks*; Springer: Berlin/Heidelberg, Germany, 2005; pp. 61–69. [[CrossRef](#)]
11. Gameda, B.T.; Lahoz, R.; Caldeira, A.T.; Schiavon, N. Efficacy of laser cleaning in the removal of biological patina on the volcanic scoria of the rock-hewn churches of Lalibela, Ethiopia. *Environ. Earth Sci.* **2018**, *77*, 36. [[CrossRef](#)]
12. Siano, S.; Salimbeni, R. Advances in Laser Cleaning of Artwork and Objects of Historical Interest: The Optimized Pulse Duration Approach. *Acc. Chem. Res.* **2010**, *43*, 739–750. [[CrossRef](#)]
13. Kearns, A.; Fischer, C.; Watkins, K.; Glasmacher, M.; Kheyrandish, H.; Brown, A.; Steen, W.; Beahan, P. Laser removal of oxides from a copper substrate using Q-switched Nd:YAG radiation at 1064 nm, 532 nm and 266 nm. *Appl. Surf. Sci.* **1998**, 127–129, 773–780. [[CrossRef](#)]
14. Chen, G.X.; Kwee, T.J.; Tan, K.P.; Choo, Y.S.; Hong, M.H. Laser cleaning of steel for paint removal. *Appl. Phys. A* **2010**, *101*, 249–253. [[CrossRef](#)]
15. Sanz, M.; Oujja, M.; Ascaso, C.; Pérez-Ortega, S.; Souza-Egipsy, V.; Fort, R.; Rios, A.D.L.; Wierzchos, J.; Cañamares, M.; Castillejo, M. Influence of wavelength on the laser removal of lichens colonizing heritage stone. *Appl. Surf. Sci.* **2017**, *399*, 758–768. [[CrossRef](#)]
16. Yandrisevits, M.A.; Londero, P.; Carò, F.; Rizzo, A.; Cappuccini, C. Wavelength-dependent absorption and scattering effects on laser cleaning of a corroded iron alloy European scale armor. In *Lasers in the Conservation of Artworks XI, Proceedings of the LACONA XI, Krakow, Poland, 20–23 September 2016*; Targowski, P., Walczak, M., Pouli, P., Eds.; NCU Press: Toruń, Poland, 2017. [[CrossRef](#)]
17. Fotakis, C.; Kautek, W.; Castillejo, M. *Lasers in the Preservation of Cultural Heritage*; CRC Press: Boca Raton, FL, USA, 2006. [[CrossRef](#)]
18. Siano, S. Principles of Laser Cleaning in Conservation. In *Handbook on the Use of Lasers in Conservation and Conservation Science*; COST G7 (2007); COST OFFICE: Brussels, Belgium, 2007; Volume 7, pp. 1–26.
19. Pouli, P.; Papanikolaou, E.; Frantzikinaki, K.; Panou, A.; Frantzi, G.; Vasiliadis, C.; Fotakis, C. The two-wavelength laser cleaning methodology; theoretical background and examples from its application on CH objects and monuments with emphasis to the Athens Acropolis sculptures. *Herit. Sci.* **2016**, *4*, 1. [[CrossRef](#)]
20. Svendsen, W.E.; Schou, J.; Thestrup, B.; Ellegaard, O. Ablation from metals induced by visible and UV laser irradiation. *Appl. Surf. Sci.* **1996**, 96–98, 518–521. [[CrossRef](#)]
21. Keller, U. Recent developments in compact ultrafast lasers. *Nature* **2003**, *424*, 831–838. [[CrossRef](#)]
22. Salimbeni, R.; Pini, R.; Siano, S. A variable pulse width Nd:YAG laser for conservation. *J. Cult. Herit.* **2003**, *4*, 72–76. [[CrossRef](#)]
23. Oujja, M.; Sanz, M.; Rebollar, E.; Marco, J.; Domingo, C.; Pouli, P.; Kogou, S.; Fotakis, C.; Castillejo, M. Wavelength and pulse duration effects on laser induced changes on raw pigments used in paintings. *Spectrochim. Acta Part A Mol. Biomol. Spectrosc.* **2012**, *102*, 7–14. [[CrossRef](#)] [[PubMed](#)]
24. Oujja, M.; García, A.; Romero, C.; de Aldana, J.R.V.; Moreno, P.; Castillejo, M. UV laser removal of varnish on tempera paintings with nanosecond and femtosecond pulses. *Phys. Chem. Chem. Phys.* **2011**, *13*, 4625–4631. [[CrossRef](#)] [[PubMed](#)]
25. Walczak, M.; Oujja, M.; Crespo-Arcá, L.; García, A.; Méndez, C.; Moreno, P.; Domingo, C.; Castillejo, M. Evaluation of femtosecond laser pulse irradiation of ancient parchment. *Appl. Surf. Sci.* **2008**, *255*, 3179–3183. [[CrossRef](#)]
26. Yakovlev, E.; Shandybina, G.; Shamova, A. Modelling of the heat accumulation process during short and ultrashort pulsed laser irradiation of bone tissue. *Biomed. Opt. Express* **2019**, *10*, 3030–3040. [[CrossRef](#)]
27. Vasantgadkar, N.A.; Bhandarkar, U.V.; Joshi, S. A finite element model to predict the ablation depth in pulsed laser ablation. *Thin Solid Films* **2010**, *519*, 1421–1430. [[CrossRef](#)]
28. Le Harzic, R.; Breitling, D.; Weikert, M.; Sommer, S.; Föhl, C.; Valette, S.; Donnet, C.; Audouard, E.; Dausinger, F. Pulse width and energy influence on laser micromachining of metals in a range of 100fs to 5ps. *Appl. Surf. Sci.* **2005**, *249*, 322–331. [[CrossRef](#)]

29. Gamaly, E. The physics of ultra-short laser interaction with solids at non-relativistic intensities. *Phys. Rep.* **2011**, *508*, 91–243. [[CrossRef](#)]
30. Pouli, P.; Paun, I.-A.; Bounos, G.; Georgiou, S.; Fotakis, C. The potential of UV femtosecond laser ablation for varnish removal in the restoration of painted works of art. *Appl. Surf. Sci.* **2008**, *254*, 6875–6879. [[CrossRef](#)]
31. Rode, A.; Baldwin, K.; Wain, A.; Madsen, N.; Freeman, D.; Delaporte, P.; Luther-Davies, B. Ultrafast laser ablation for restoration of heritage objects. *Appl. Surf. Sci.* **2007**, *254*, 3137–3146. [[CrossRef](#)]
32. Lippert, T.; Dickinson, J.T. Chemical and Spectroscopic Aspects of Polymer Ablation: Special Features and Novel Directions. *Chem. Rev.* **2003**, *103*, 453–486. [[CrossRef](#)] [[PubMed](#)]
33. Paraskevi, P.; Alexandros, S.; Savas, G.; Fotakis, C. Recent Studies of Laser Science in Paintings Conservation and Research. *Acc. Chem. Res.* **2010**, *43*, 771–781.
34. Di Niso, F.; Gaudiuso, C.; Sibillano, T.; Mezzapesa, F.P.; Ancona, A.; Lugarà, P.M. Role of heat accumulation on the incubation effect in multi-shot laser ablation of stainless steel at high repetition rates. *Opt. Express* **2014**, *22*, 12200–12210. [[CrossRef](#)]
35. Mensink, K.; Penilla, E.H.; Martínez-Torres, P.; Cuando, N.; Mathaudhu, S.; Aguilar, G. High repetition rate femtosecond laser heat accumulation and ablation thresholds in cobalt-binder and binderless tungsten carbides. *J. Mater. Process. Technol.* **2018**, *266*, 388–396. [[CrossRef](#)]
36. Phillips, K.C.; Gandhi, H.H.; Mazur, E.; Sundaram, S.K. Ultrafast laser processing of materials: A review. *Adv. Opt. Photonics* **2015**, *7*, 684–712. [[CrossRef](#)]
37. Marczak, J.; Koss, A.; Targowski, P.; Góra, M.; Strzelec, M.; Sarzyński, A.; Skrzeczanowski, W.; Ostrowski, R.; Rycyk, A. Characterization of Laser Cleaning of Artworks. *Sensors* **2008**, *8*, 6507–6548. [[CrossRef](#)] [[PubMed](#)]
38. Žemaitis, A.; Gaidys, M.; Brikas, M.; Gečys, P.; Račiukaitis, G.; Gedvilas, M. Advanced laser scanning for highly-efficient ablation and ultrafast surface structuring: Experiment and model. *Sci. Rep.* **2018**, *8*, 17376. [[CrossRef](#)] [[PubMed](#)]
39. Liu, K.; Garmire, E. Paint removal using lasers. *Appl. Opt.* **1995**, *34*, 4409–4415. [[CrossRef](#)]
40. Liu, X.; Du, D.; Mourou, G. Laser ablation and micromachining with ultrashort laser pulses. *IEEE J. Quantum Electron.* **1997**, *33*, 1706–1716. [[CrossRef](#)]
41. Gunness, B. Laser cleaning. *Corros. Mater.* **2018**, *43*, 46–47. [[CrossRef](#)]
42. Chichkov, B.N.; Momma, C.; Nolte, S.; Von Alvensleben, F.; Tünnermann, A. Femtosecond, picosecond and nanosecond laser ablation of solids. *Appl. Phys. A* **1996**, *63*, 109–115. [[CrossRef](#)]
43. Pouli, P.; Oujja, M.; Castillejo, M. Practical issues in laser cleaning of stone and painted artefacts: Optimisation procedures and side effects. *Appl. Phys. A* **2011**, *106*, 447–464. [[CrossRef](#)]
44. Al Sekhaneh, W.; El Serogy, A.; El-Bakri, M. Yag-Laser Cleaning of Archaeological Materials in Jordanian Museums. *Mediterr. Archaeol. Archaeom.* **2015**, *15*, 157–164. [[CrossRef](#)]
45. Bilmes, G.M.; Freiszstav, C.; Schinca, D.; Orsetti, A. Cleaning and characterization of objects of cultural value by laser ablation. In *Optical Methods for Arts and Archaeology*; SPIE: Bellingham, WA, USA, 2005; Volume 5857, p. 585704. [[CrossRef](#)]
46. Carbonell, E.; De Castro, J.M.B.; Parés, J.M.; Pérez-González, A.; Cuenca-Bescós, G.; Ollé, A.; Mosquera, M.; Huguet, R.; Van Der Made, J.; Rosas, A.; et al. The first hominin of Europe. *Nature* **2008**, *452*, 465–469. [[CrossRef](#)]
47. Arsuaga, J.L.; Martínez, I.; Gracia, A.; Carretero, J.-M.; Lorenzo, C.; García, N.; Ortega, A.I. Sima de los Huesos (Sierra de Atapuerca, Spain). The site. *J. Hum. Evol.* **1997**, *33*, 109–127. [[CrossRef](#)]
48. Caldararo, N. Effects of cleaning and regard for cleaning goals: Eleven years later. *AIC Objects Spec. Group Postprints* **2005**, *12*, 126–153.
49. Rahman, M.A. Laser Based Intervention in Archaeological Materials and Museum Artifacts. Ph.D. Thesis, University of Burgos, Burgos, Spain, University of Évora, Évora, Portugal, 2022.
50. Bischoff, J.; Fitzpatrick, J.; León, L.; Arsuaga, J.; Falgueres, C.; Bahain, J.; Bullen, T. Geology and preliminary dating of the hominid-bearing sedimentary fill of the Sima de los Huesos Chamber, Cueva Mayor of the Sierra de Atapuerca, Burgos, Spain. *J. Hum. Evol.* **1997**, *33*, 129–154. [[CrossRef](#)] [[PubMed](#)]
51. Suarez, C.A.; Morschhauser, E.M.; Suarez, M.B.; You, H.; Li, D.; Dodson, P. Rare earth element geochemistry of bone beds from the Lower Cretaceous Zhonggou Formation of Gansu Province, China. *J. Vertebr. Paléontol.* **2018**, *38*, 22–35. [[CrossRef](#)]
52. Liu, J.M. Simple technique for measurements of pulsed Gaussian-beam spot sizes. *Opt. Lett.* **1982**, *7*, 196–198. [[CrossRef](#)]
53. Rode, A.V.; Freeman, D.; Baldwin, K.G.H.; Wain, A.; Uteza, O.; Delaporte, P. Scanning the laser beam for ultrafast pulse laser cleaning of paint. *Appl. Phys. A* **2008**, *93*, 135–139. [[CrossRef](#)]
54. Absolonová, K.; Dobisiková, M.; Beran, M.; Zocová, J.; Velemínský, P. The temperature of cremation and its effect on the microstructure of the human rib compact bone. *Anthr. Anz.* **2012**, *69*, 439–460. [[CrossRef](#)]
55. Bäuerle, D. Thermal, Photophysical, and Photochemical Processes. In *Laser Processing and Chemistry*; Springer: Berlin/Heidelberg, Germany, 2000; pp. 13–38. [[CrossRef](#)]
56. Maingi, E.M.; Alonso, M.P.; Angurel, L.A.; Rahman, A.; Chapoulie, R.; Dubernet, S.; de la Fuente, G.F. Historical stained-glass window laser preservation: The heat accumulation challenge. *Bol. Soc. Esp. Ceram. Vid.* **2022**, *61* (Suppl.1), S69–S82. [[CrossRef](#)]
57. Gutiérrez, A.M.; Ruiz, M.N.; Barredo, F.J. Estudio experimental acerca de la pátina que adquieren los materiales de sílex neógeno procedente de la sierra de Atapuerca. *Arqueol. Del. Paleolítico.* **2017**, *5*, 35–52.
58. Della Pepa, G. Microelements for bone boost: The last but not the least. *Bone Abstr.* **2016**, *13*, 181–185. [[CrossRef](#)]

59. Sasso, G.D.; Lebon, M.; Angelini, I.; Maritan, L.; Usai, D.; Artioli, G. Bone diagenesis variability among multiple burial phases at Al Khiday (Sudan) investigated by ATR-FTIR spectroscopy. *Palaeogeogr. Palaeoclim. Palaeoecol.* **2016**, *463*, 168–179. [[CrossRef](#)]
60. Chang, M.C.; Tanaka, J. FT-IR study for hydroxyapatite/collagen nanocomposite cross-linked by glutaraldehyde. *Biomaterials* **2002**, *23*, 4811–4818. [[CrossRef](#)] [[PubMed](#)]
61. Canguero, L.T.; Vilar, R.M.C.S.; do Rego, A.M.B.; Muralha, V.S.F. Femtosecond laser ablation of bovine cortical bone. *J. Biomed. Opt. Vol.* **2012**, *17*, 125005. [[CrossRef](#)] [[PubMed](#)]
62. Rehman, I.; Bonfield, W. Characterization of hydroxyapatite and carbonated apatite by photo acoustic FTIR spectroscopy. *J. Mater. Sci. Mater. Med.* **1997**, *8*, 1–4. [[CrossRef](#)] [[PubMed](#)]
63. Eugénio, S.; Sivakumar, M.; Vilar, R.; Rego, A.M. Characterisation of dentin surfaces processed with KrF excimer laser radiation. *Biomaterials* **2005**, *26*, 6780–6787. [[CrossRef](#)] [[PubMed](#)]

Disclaimer/Publisher’s Note: The statements, opinions and data contained in all publications are solely those of the individual author(s) and contributor(s) and not of MDPI and/or the editor(s). MDPI and/or the editor(s) disclaim responsibility for any injury to people or property resulting from any ideas, methods, instructions or products referred to in the content.